TSUNAMI INUNDATION MODELING: SENSITIVITY OF VELOCITY AND MOMENTUM FLUX TO BOTTOM FRICTION WITH APPLICATION TO BUILDING DAMAGE AT SEASIDE, OREGON

Hyoungsu Park[1], Dane Wiebe[2], Daniel Cox[3], and Katherine Cox[4]

We examine the sensitivity of three different tsunami inundation numerical models using various friction terms. We use the model output to examine the probabilistic damage levels using fragility curves applied over a community scale and resolved at the scale of individual tax lots for Seaside, OR. With this work, we estimate the inundation hazard using the "500 year" tsunami originating from a Cascadia Subduction Zone earthquake and then compare the maximum surface elevation, velocity, and momentum flux results across the three models. We find a larger variation in the velocities and momentum fluxes when varying model types and friction coefficients; surface elevation variations are not as large. We also find that absolute velocity and momentum flux are more sensitive to friction factors rather than model type, while surface elevation varies with model type. For the fragility curve analysis, we consider flow depth, velocity, and momentum flux as the intensity measure to estimate the probability of a certain damage level based on the known structure type and characteristic tsunami intensity. We examine the sensitivity of damage levels to various fragility curves, using different intensity measures, and we find that velocity and momentum flux curves provide a more realistic estimate of damage.

Keywords: tsunami inundation; numerical modeling; fragility curve; Cascadia Subduction Zone; ADCIRC; Coulwave; ComMIT/MOST; Seaside

Introduction

Tsunami modeling has matured over the past several decades and now provides reliable estimates of the tsunami arrival time, the time-varying water levels during inundation, and the maximum extent of inundation among other things. These models can provide coastal communities with necessary information for evacuation planning, especially if the objective is complete evacuation from the inundation area (horizontal evacuation). However, it is not clear whether these models provide accurate estimates of the fluid velocity and momentum flux within the inundation zone. This is problematic for engineers who want to design shelter-in-place options (vertical evacuation) or coastal planners who want to estimate the extent of damage to the built environment on community and regional scales. Part of this uncertainty arises from a simplification during the inundation phase; energy losses are estimated using an empirical bottom friction coefficient. While water levels predicted by tidal circulation models are relatively insensitive to friction factor choices, the same cannot be said of velocity. For tsunami inundation, which has time and length scales comparable to those for storm surge and tides, we anticipate that inundation velocity predictions are sensitive to bottom friction and may lead to large uncertainties in hydraulic forces for engineering design.

To test this hypothesis, we conducted a numerical model study using three well-known models: ComMIT/MOST, ADCIRC, and Coulwave. We considered the scenario of a tsunami produced by a large earthquake along the Cascadia Subduction Zone, and we focused on inundation at Seaside, Oregon, because it has been well documented in other studies. We used ComMIT/MOST to generate the tsunami source and a series of nested grids to propagate the tsunami nearshore. We then used the ComMIT/MOST model output as a common seaward boundary condition for the other two models. We ran four different friction factors with each model, and we compared the free surface, velocity and momentum flux at several cross-shore locations. We used the work of Wiebe and Cox (2014) to estimate the corresponding damage level assuming the buildings were either wooden houses or steel-reinforced concrete. We applied three different types of fragility curves for over 20,000 buildings in the Seaside area to show the overall sensitivity of total building damage to variations in the fragility curves (maximum flow depth, velocity and momentum flux).

Numerical model simulation

Seaside, OR, is one of the most vulnerable coastal cities in the Pacific Northwest United States given the threat of an extreme nearfield Cascadia Subduction Zone earthquake and resulting tsunami. Prior

[1] School of Civil and Construction Engineering, Oregon State University, Corvallis, OR 97331 USA
[2] Applied Science, Inc, Detroit, MI USA
[3] School of Civil and Construction Engineering, Oregon State University, Corvallis, OR 97331 USA
[4] Corvallis, OR 97330 USA

tsunami related research has estimated maximum runup and arrival time for various tsunami scenarios in this area, including damage level estimates and general guidelines to mitigate future tsunamis (Tsunami Pilot Study Working Group, 2006; Gonzalez et al., 2009; Wiebe and Cox, 2014).

In our study, we focused on the sensitivity of numerical simulations using three different model types and specified friction coefficients. We also tested sensitivity of damage levels using various fragility curves. We compared three well-known inundation models: ComMIT/MOST, Coulwave, and ADCIRC. ComMIT/MOST is the tsunami model of NOAA Center for Tsunami Research (NCTR), which is applied for warning forecasts and tsunami inundation mapping. The Method of Splitting Tsunami (MOST) model has been verified with various bench marking tests and laboratory experiments (Synolaiks et al., 2008). Coulwave (Lynett et al., 2002) solves a set of Boussinesq equations and includes bottom friction effects with a high-order finite-volume method. Coulwave has been validated with fundamental benchmark problems for runup using field data and experimental data (Lynett et al., 2002; Lynett and Liu, 2005; Park et al., 2013). ADCIRC (Luettich and Westerink, 2004) solves the non-linear shallow equation using a finite element method and is widely utilized for hurricane wave inundation problems when coupled with SWAN. ADCIRC is well verified with field buoy data or hurricane inundation observations, but it is not frequently used to simulate tsunami inundation. In this study we provided the same boundary conditions to Coulwave and ADCIRC and compared results in terms of free surface, velocity and momentum flux inside the inundation zone.

We used ComMIT/MOST, which includes a tsunami source term, to generate hypothetical tsunamis at the Cascadia Subduction Zone (CSZ), and a nested grid to propagate each tsunami shoreward. We utilized the output of the second nested grid for the third nested grid and as a common seaward boundary condition for Coulwave and ADCIRC. Figure 1 shows images of our study area and the nested grids, and Table 1 lists details of the numerical model grid (ComMIT/MOST) information. ComMIT/MOST model grids comprise three series of nested grids (A, B, and C) to optimize the model simulation for three tsunami processes: generation, propagation and inundation. The grid sizes of A, B, and C are 36, 4, and 1 sec. In addition to ComMIT/MOST, we also examine Coulwave and ADCIRC to test the sensitivity between inundation model types. The grid size for Coulwave is 30 m, and the ADCIRC grid is between 20 to 100 m. Grid size details are also listed in Table. 1.

Figure 2 shows four hypothetical tsunami inputs for the innermost grid (C') shown in Figure 1(b); the tsunami data are extracted from ComMIT/MOST. We assume the tsunami occurs from full slip conditions at the CSZ, with slip values from 5 to 14 m, and chose realistic earthquake magnitudes ranging from Mw = 8.8 to 9.1. There is about a 10% chance of a 9.0 Mw earthquake at the CSZ over a 35 year timeframe, therefore we used Mw = 9.0 (10 m slip condition) as a default hypothetical tsunami input in this study (e.g., Goldfinger et al., 2009).

Figure 3 illustrates the detailed bathymetry for Grid C' at Seaside. The bathymetry was generated with the NOAA Center for Tsunami Research file titled “Seaside, 1/3 arc-second, 2004-04-01,” http://www.ngdc.noaa.gov/mgg/inundation. The contours are relative to the mean high water level (MHW). We fixed a constant tide level as MHW during the hypothetical tsunami process.
The center dotted line (CL) in Figure 3 indicates the cross-shore observation line. Nine observation points were selected with 4 points seaward of the shoreline, and 5 points landward. These locations were used to compare the tsunami characteristics of flow depth or surface elevation (offshore and onshore, respectively), velocity, momentum flux, and arrival time.

Figure 4 shows the cross-shore bathymetry profiles and maximum elevations along the centerline (CL in Figure 3) for the default hypothetical tsunami scenario. The onshore bathmetry/topography profile crosses the Necanicum River and Neawanna Creek and can be seen as negative land elevations behind the dune. Seaside shows a relatively plain slope in the onshore direction after the dune at the shoreline. We find that the cross-shore bathymetry profiles across the three models show good agreement while the maximum elevations show less variation before the shoreline ($x = 0$) and slighly more variation in the inundation area ($x > 0$) due to model type. Nevertheless, the models can be considered to have the same bathymetry.

Table 1: Grid sizes and dimensions for comparative model study.

	A – grid (MOST)	B – grid (MOST)	C – grid (MOST)	C' – grid (COULWAVE)	C' – grid (ADCIRC)
Grid size	36 sec	4 sec	1 sec	30 m (~ 1sec)	20 m ~ 100 m
Dimension	400 x 400	800 x 800	531 X 645	430 X 320	103,805

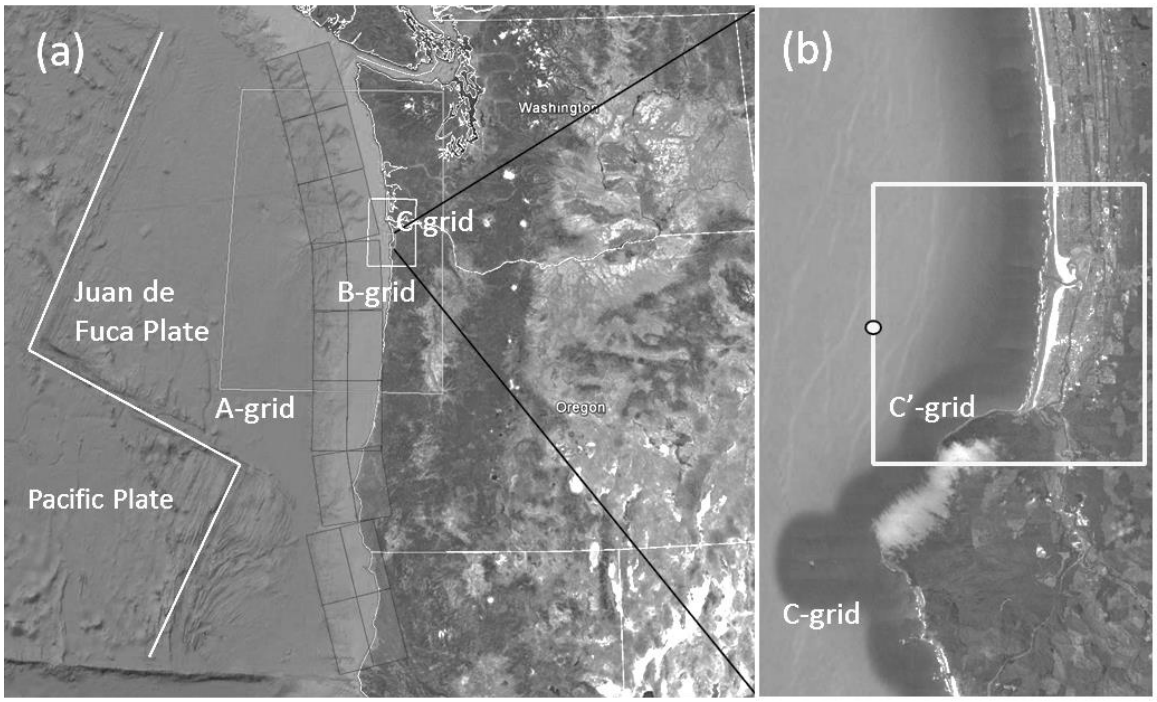

Figure 1: Image of study area (a) and details of numerical model grids (b) for Seaside, Oregon.

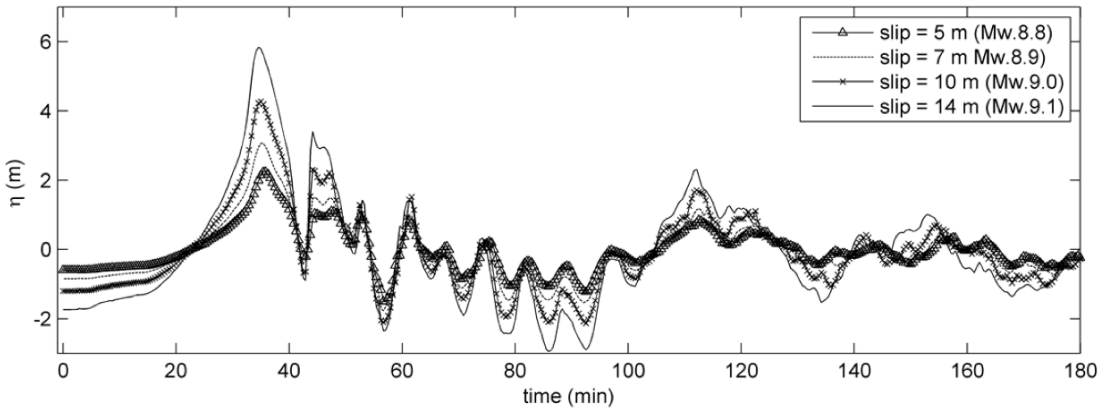

Figure 2: Hypothetical tsunami input for a Cascadia Subduction Zone event from ComMIT/MOST and used as input to the numerical models.

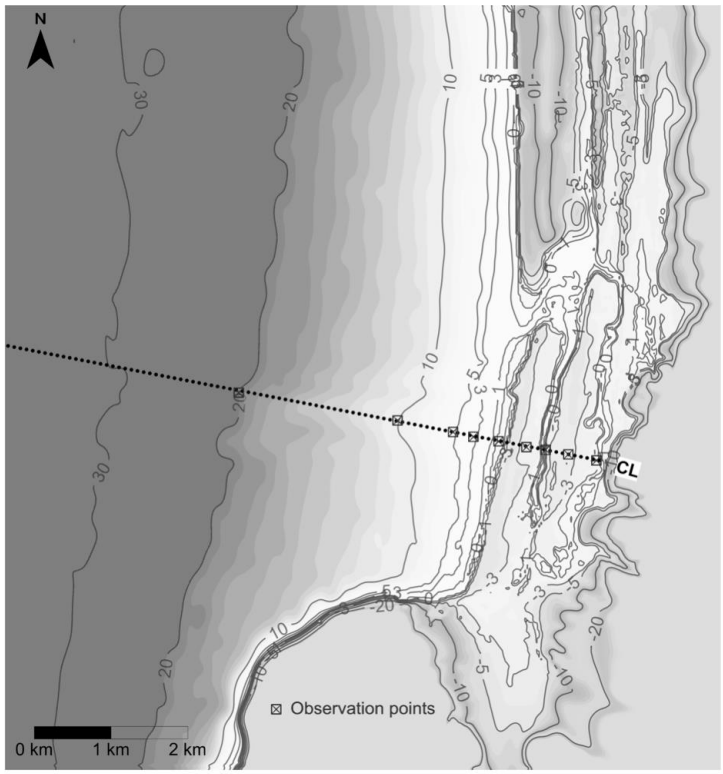

Figure 3: Bathymetry detail of Grid C at Seaside, Oregon. The dotted line indicates the centerline transect used for model comparison.

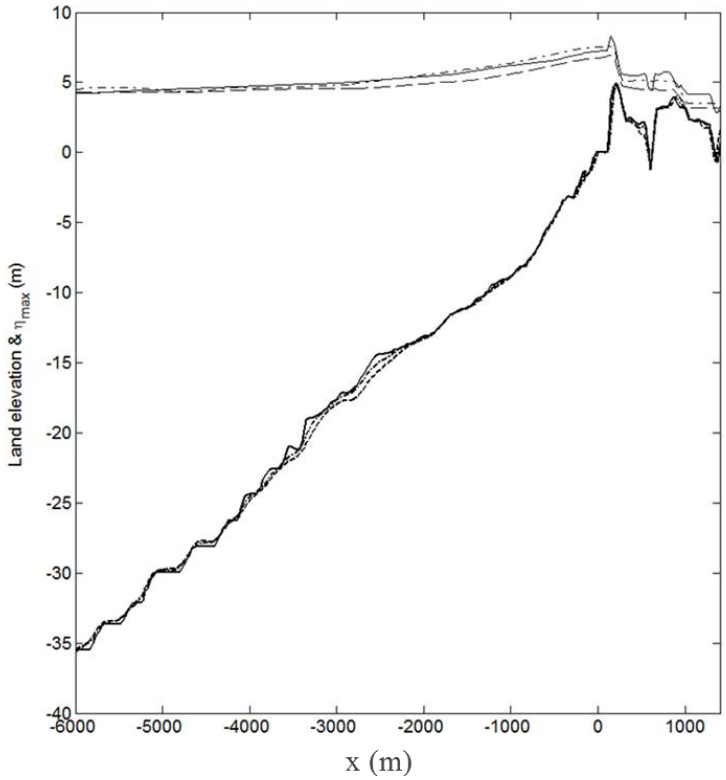

Figure 4: Inter-model comparison of cross-shore bathymetry profiles and maximum elevations along centerline. ComMIT/MOST (solid), Coulwave (dash-dot) and ADCIRC (dash).

Figure 5 provides a more detailed comparison in the inundation area. Figure 5a presents the maximum free surface elevations for the three numerical models. The thick elevation line in Figure 5a illustrates the cross-shore bathymetry profile of ComMIT/MOST. Figure 5b shows the maximum velocitiy calcualted as the root square sum of the x and y velocity components. Figure 5c shows the maximum momentum flux calculated as the product of velocity squared and the local flow depth taken as the surface elevation minus the local land elevation.

Near the shoreline (x = 0), the maximum surface elevations are similar and close to 7 m but then deviate as water inundates land. Coulwave (dash-dot) and ADCIRC (dash) show a similar pattern, but the MOST(solid) model result is more conservative. For the case of maximum velocity and momentum flux, the results are different across the entire inundation region including the shoreline. More variation occurs at maximum momentum flux because the momentum flux includes terms with velocity squared. We find again that Coulwave and ADCIRC show similar patterns, the MOST model results are generally conservative, and the momentum flux estimates are often larger by a factor of 2 or 3 compared to the Coulwave and ADCIRC results.

Figure 6 presents the maximum values for (a) surface elevation, (b) velocity, and (c) momentum flux for various friction coefficients (Manning number) for the MOST model with n = 0.02 (solid), 0.03 (dash-dot), 0.04 (dash), and 0.05 (dot) along the CL. Overall, as friction increases all values decrease. A relatively small difference is found between the maximum surface elevations (Fig. 6a), but greater variations are found with maximum velocity (Fig. 6b) and maximum momentum flux (Fig. 6c). These results highlight that, in the inundation area, the maximum velocity and momentum flux are more sensitive to friction than the maximum elevation is.

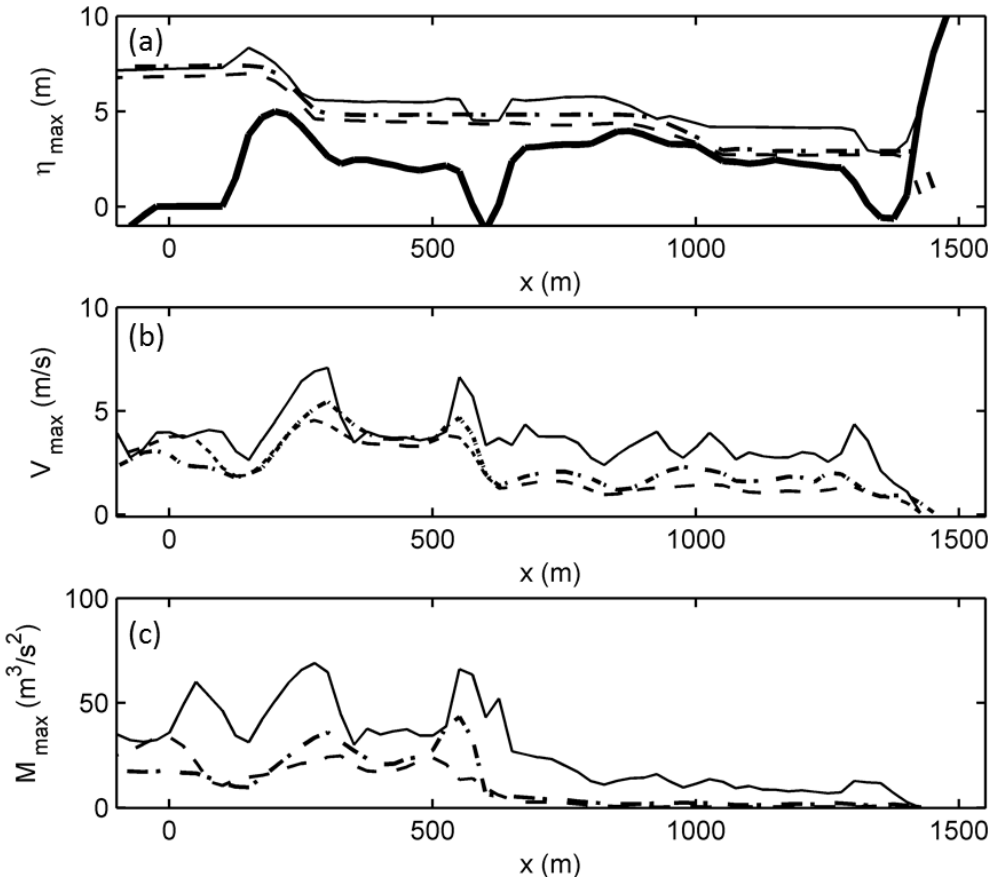

Figure 5: Inter-model comparison of (a) maximum free surface elevation, (b) velocity and (c) momentum flux along the centerline. The still water shoreline occurs at x=0. MOST (solid), Coulwave (dash-dot) and ADCIRC (dash).

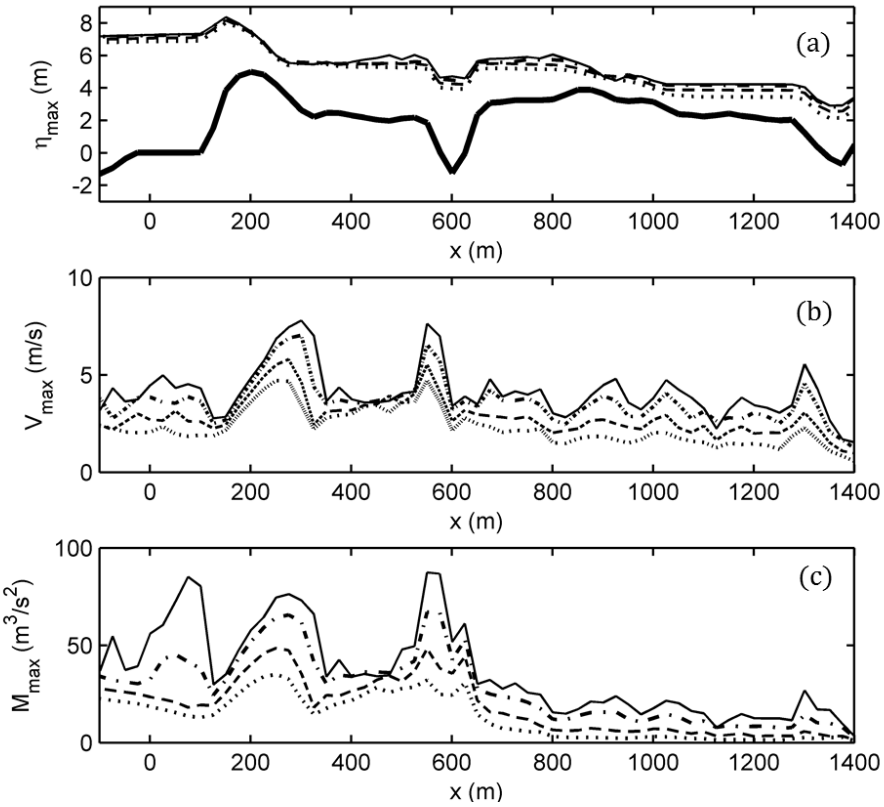

Figure 6: Sensitivity to friction coefficient (Manning number) for the MOST model of (a) maximum free surface elevation, (b) maximum velocity and (c) maximum momentum flux along the centerline with n=0.02 (solid), n=0.03 (dash-dot), n=0.04 (dash), and n = 0.05 (dotted).

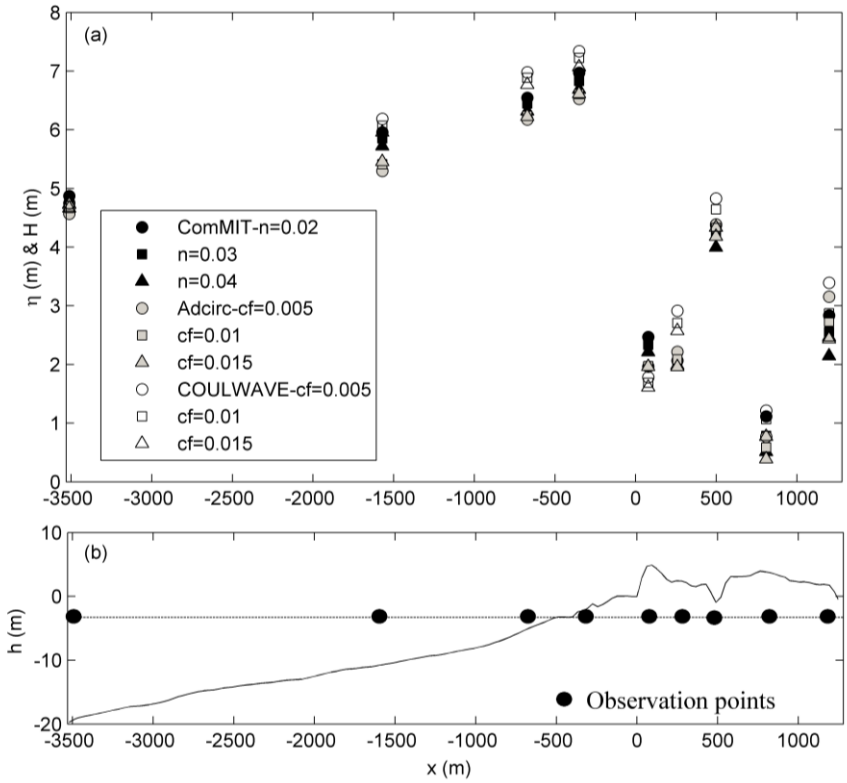

Figure 7: Sensitivity of maximum free surface elevation to changes in bottom friction at several observation points along the centerline.

Figure 7a shows the sensitivity of maximum surface elevations (x < 0) or flow depth (x > 0) for the different models with various friction coefficients. The x-axis shows the distance from the shore line. Figure 7b presents the location of 9 observation points along the CL.

Figure 8 illustrates the sensitivity of (a) the maximum velocity and (b) momentum flux for the three different models using various friction coefficients during inundation (x>0). We find the largest variation in velocity and momentum flux occurs at x ~ 220 m, where the maximum velocity and momentum flux values are 4 and 5 times greater than the smallest ones. Also, the absolute velocity and momentum flux varies more with different friction conditions than with model type, which is the opposite of what occurred with surface elevations in Figure 7a.

Figure 9 presents the arrival time of the maximum surface elevation for the different models using the same friction conditions as in the previous Figures. The y-axis indicates the time (min) after a tsunami is triggered at the CSZ until the maximum surface elevation is observed at the observation points. We find that offshore the arrival times are consistent across models and friction values until the shoreline locations (x ~ 50 m). Over land, the variation in arrival times increases as the distance landward increases. Note that the arrival time values in Figure 9 are not the same as the arrival time of the leading positive wave. Arrival time of the nearfield CSZ tsunami is important for evacuation plans since the time to respond to a local tsunami event is relatively short.

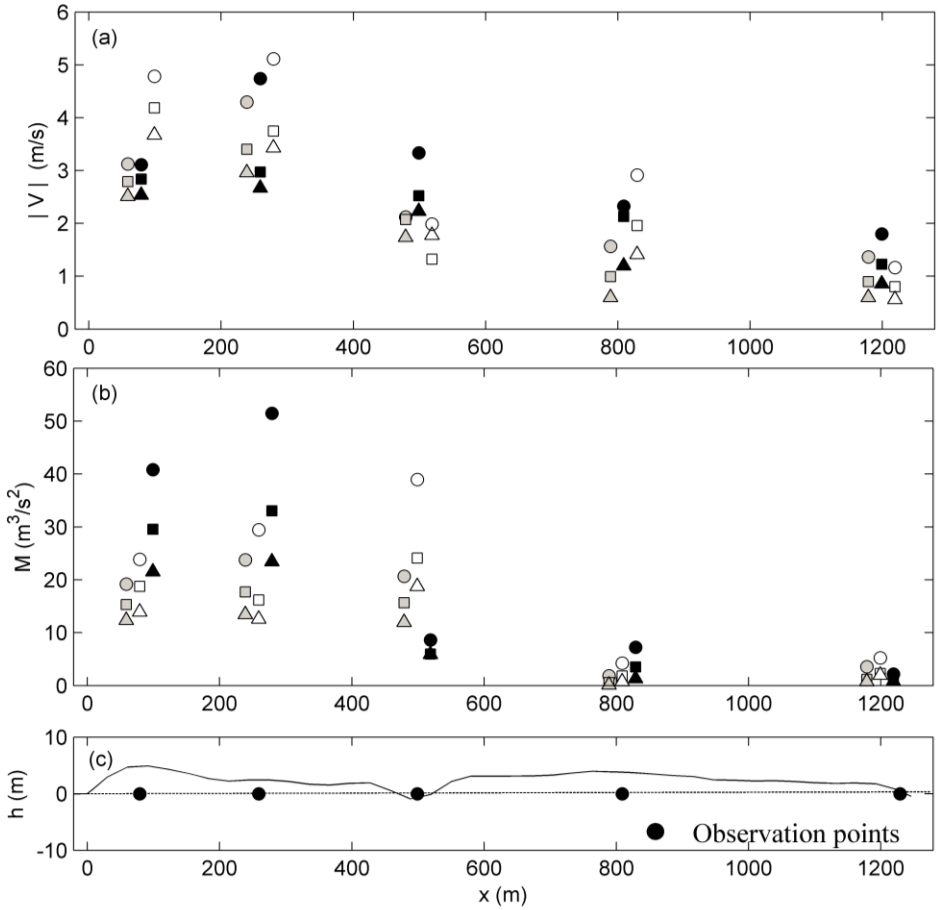

Figure 8: Sensitivity of maximum absolute velocity (upper panel) and momentum flux (middle panel) to the range of friction values shown in Figure 7. Note that in both panels the abscissa for the model output is shifted slightly at each location for visual clarity: ADCIRC (grey set of triangle, square, and circle), Coulwave (white, second set) and MOST (black, third set).

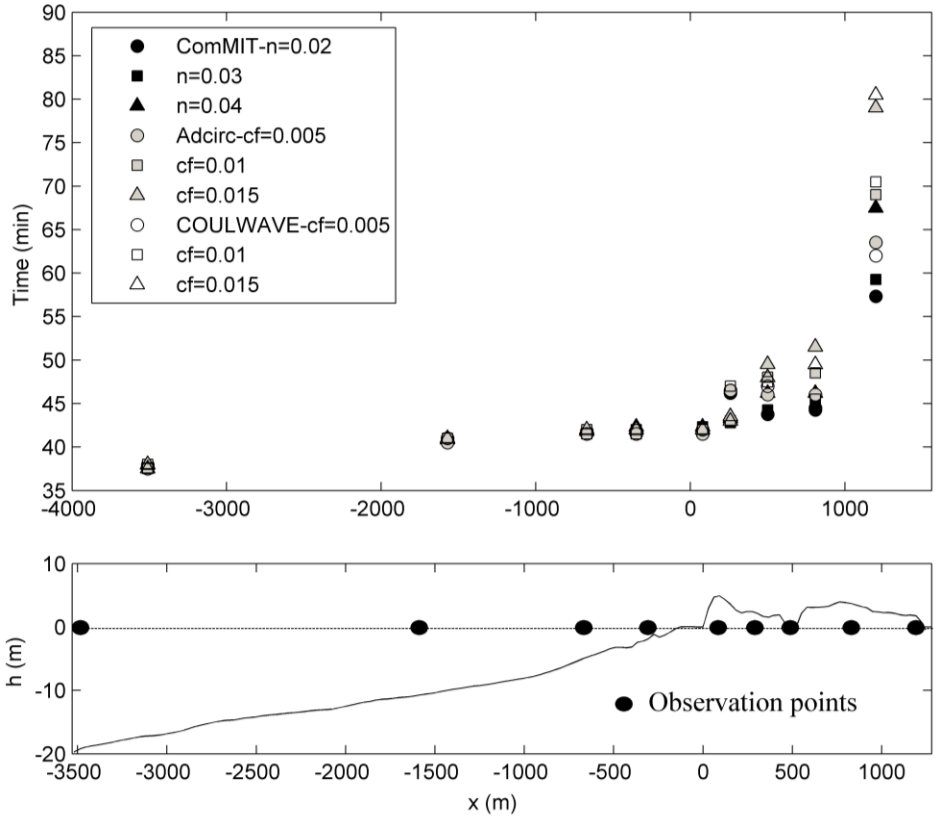

Figure 9: Sensitivity of tsunami arrival time.

Damage estimation using fragility curves

A fragility curve is an empirical approach often developed using survey data from past disasters to estimate the likelihood of a specific damage level for a particular building type as a function of a given intensity measure. For tsunami inundation, the intensity measure may be flood depth, flow speed, or momentum flux. Following the 2004 tsunami, researchers relied on before and after aerial photos to estimate damage levels to buildings coupled with corresponding hydrodynamics or numerical simulations and some field observations to estimate tsunami fragility curves (Koshimura, et al, 2009; Suppasri, et, al, 2011). After the 2011 tsunami, various research groups were organized to estimate the specific damage levels of buildings and the corresponding maximum flow depths or runups with field surveys. Based on those survey data, various fragility curves were developed for the various damage levels, structure materials, sizes, or locations (Suppasri, et al., 2013). The maximum flow depth is widely used as the intensity measure to estimate damage levels in fragility curves, despite the limitation that flow depth cannot directly represent the tsunami force. Therefore fragiliy curves from flow depth include the uncertainty of estimaitng a future tsunami hazard. Wiebe and Cox (2014) provided estimates for damage costs for a hypothetical tsunami at Seaside, OR, and they showed how fragility curves for RC and wood structures provide different insights toward damage levels and corresponding costs over the inundation area. They applied fragility curves from Suppasri et al (2013), which are only depth oriented curves.

In the second part of this study, we focus on the effects of the different types of fragility curves (flow depth, velocity, and momentum flux) including the effects of the sensitivity of velocity to the friction factor from the first part of the study. Figures 10a, b, and c show the three representative types of fragility curves from Koshimura et al. (2009) (solid line). Since there are no available fragility curves for RC structures in Koshimura et al. (2009), we calculated the fragility curves manually for RC structures based on the relationship of RC and wood structure fragility curves from Suppasri et al. (2013). Table 2 shows the ratio comparison between RC and wood structures for each type of structure and number of stories, and we used the first ratios for RC and wood structures overall (2.48 for R_μ, and 1.82 for R_σ) to create the RC fragility curves from the wood fragility curves (dotted lines) in Figure 10.

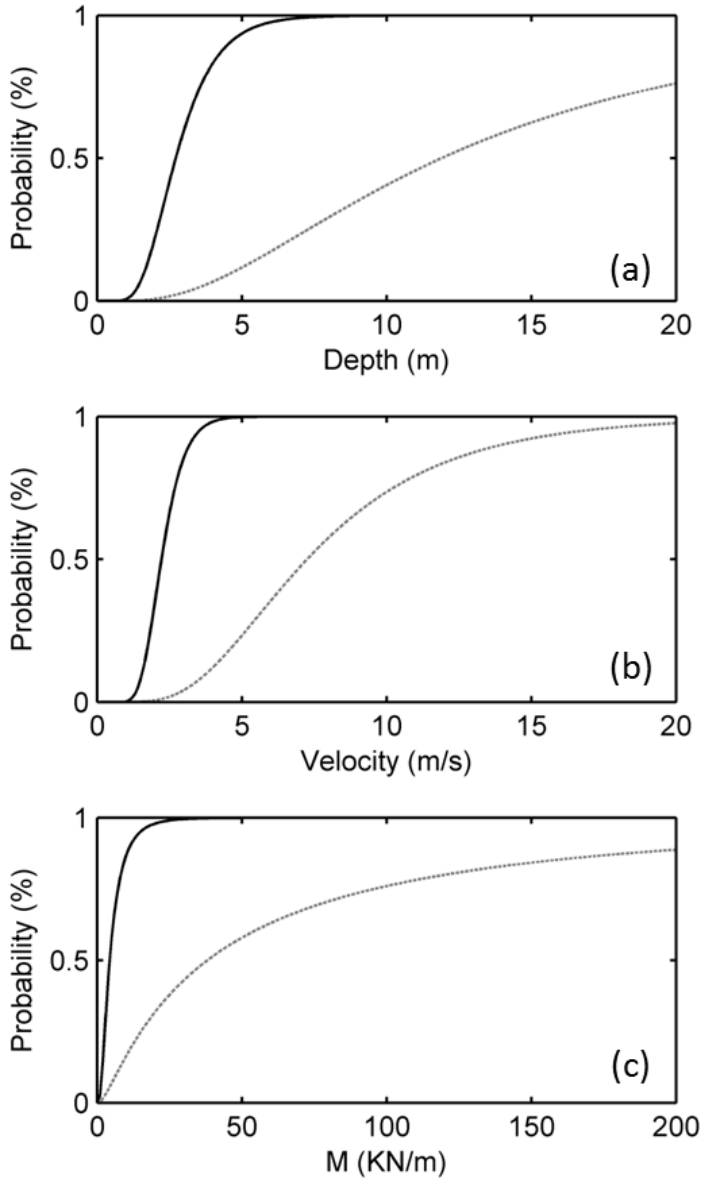

Figure 10: Fragility curves for Wood (solid) and RC buildings (dotted line) considering (a) flow depth, (b) velocity, and (c) momentum flux.

Table 2: Factors used in fragility analysis.

	μ	σ	R^2	R_μ (μ_{RC} / μ_{Wood})	R_σ (σ_{RC} / σ_{Wood})
RC	1.9381	1.0120	0.95	2.48	1.82
Wood	0.7825	0.5559	0.98		
RC 1 story	1.6578	0.8948	0.87	2.04	1.51
Wood 1 story	0.8134	0.5941	0.97		
RC 2 story	1.7814	0.7196	0.92	1.88	1.25
Wood 2 story	0.9461	0.5744	0.98		
RC 3 story	2.3491	0.7898	0.72	1.86	1.27
Wood 3 story	1.2658	0.6242	0.83		

Figure 11 shows an aerial photo of the central economic zone of Seaside from Google Earth (Figure 11a) and an approximate distribution of building types (Figure 11b). Building materials were simplified into two types: wood or RC structures. Tax lot data for Clatsop County, OR, were reviewed to determine the building type (Wiebe and Cox, 2014). The black buildings in Figure 11(b) represent RC structures. The majority of RC structures consisted of commercial buildings and hotels and are aggregated in the center of the study area near the Necanicum River; wood structures are primarily houses and are located over the entire area.

Figure 12 shows the different damage levels that resulted from model output with different fragility curves using (a) flow depth, (b) velocity, and (c) momentum flux as the intensity measure. The three different fragility curves yield results that show different damage levels for a single tsunami case (Mw = 9.0 m, MOST model with n = 0.03). The velocity (Figure 12b) and momentum flux (Figure 12c) models show a similar pattern overall, but the flow depth model results (Figure 12a) are different. The damage levels from depth fragility curves show the most severe damage concentrated near the shoreline and Necanicum River regions while the most severe damage from the velocity and momentum flux fragility curves are found over the entire region between the shoreline to the Necanicum River.

In general, severe damage will occur near the shoreline where the flow depth and velocity are significant. However, as inundation occurs, the flow loses energy from the bottom friction and the damage levels at the farthest extent of inundation are smaller. Although it is difficult to conclude without verification from field data, we observe that the velocity or momentum flux fragility curve damage results (Figures 12b and 12c) are more realistic than the depth fragility curve results based on observations of building damage patterns after the 2011 tsunami.

Discussion and Conclusion

This paper conducted a numerical model study using three well-known models: MOST, ADCIRC, and Coulwave. We considered the scenario of a tsunami generated by a large earthquake along the Cascadia Subduction Zone, and we focused on the inundation of Seaside, Oregon, We used MOST to generate the tsunami source, applying a series of nested grids to propagate the tsunami to the nearshore. We then used the MOST model output as a common seaward boundary condition for other two models. We ran four different friction factors for each model and compared the free surface, velocity, momentum flux and arrival time along a centerline (CL) transect shown in Figure 3.

Through the sensitivity tests for each model and varying friction values (Figures 7 and 8), we found that there was relatively little variation in the water levels among the three models and among the range of friction factors for a given model. On the other hand, we found large variations in the velocities and momentum fluxes due to model type and friction coefficients used. We found that the absolute velocity and momentum flux were more sensitive to friction factors than to model type, which is the opposite of what occurred with the maximum surface elevations. Additionally, arrival time of the maximum surface elevation was not sensitive to the model type or friction factor used seaward of the shoreline ($x < 0$). Landward of the shoreline, the arrival time of the maximum level was sensitive to the friction factor (Figure 9).

Following the work of Wiebe and Cox (2014), we estimated building damage levels in Seaside, OR (Figure 12) using three different types of fragility curves (maximum flow depth, velocity, and momentum flux). Among the three probability damage maps, velocity and momentum flux fragility curves were shown to be more realistic when compared to the flow depth fragility curves.

ACKNOWLEDGMENTS

This research is based upon work partially supported by Oregon Sea Grant (R/CNH-22). Any opinions, findings, and conclusions or recommendations expressed in this document are those of the authors and do not necessarily reflect the views of Oregon Sea Grant.

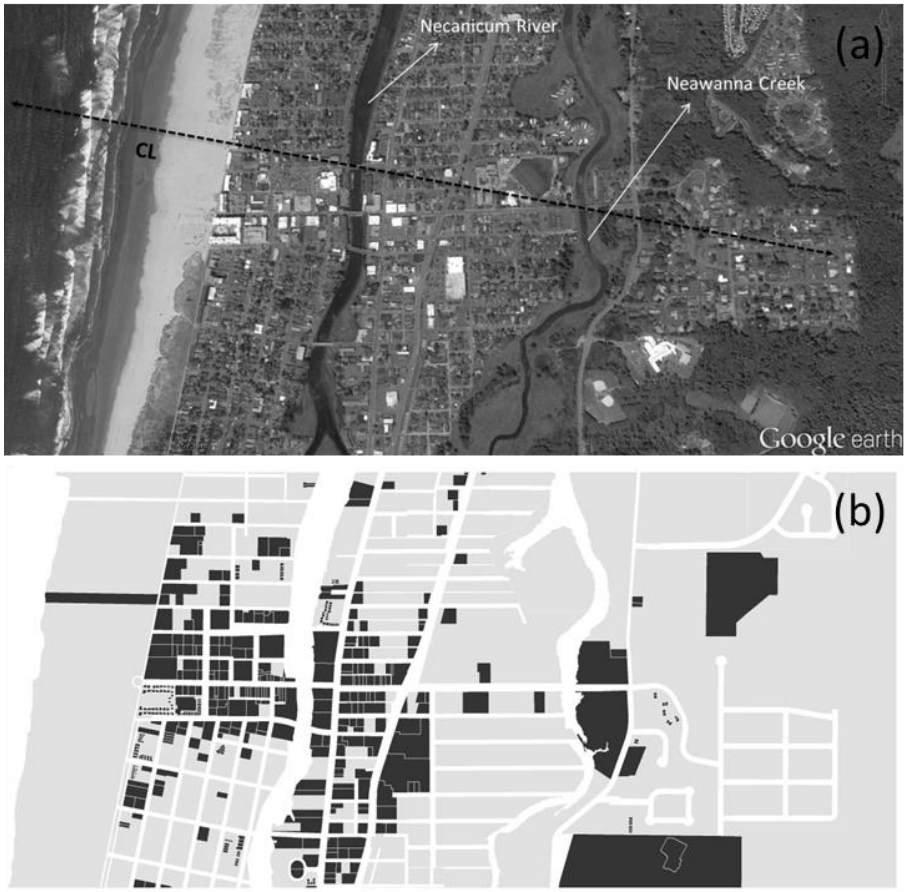

Figure 11: (a) Aerial image of Seaside and (b) distribution of building type (black = RC structures).

Figure 12: Probability damage maps using fragility functions based on (a) depth, (b) velocity, and (c) momentum flux.

REFERENCES

Goldfinger C, Nelson CH, Morey AE, Johnson JE, Patton JR, Karabanov E et al (2012) Turbidite event history—methods and implications for holocene paleoseismicity of the Cascadia subduction zone. U.S. Geological Survey Professional Paper 1661–F, 170 p

Gonzalez FI, Geist EL, Jaffe B, Kanoglu U, Mofjeld H, Synolakis CE et al (2009) Probabilistic tsunami hazard assessment at Seaside, Oregon, for near- and far-field seismic sources. J Geophys Res 114:1–19

Koshimura S, Oie T, Yanagisawa H, Imanura F (2009) Developing fragility functions for tsunami damage estimation using numerical model and post-tsunami data from Banda Aceh, Indonesia. Coast Eng J51:243–273

Luettich, R. A., & Westerink, J. J. (2004). *Formulation and numerical implementation of the 2D/3D ADCIRC finite element model version 44. XX* (p. 74).

Lynett, P. and Liu, P. L.-F (2005) A Numerical Study of the Runup Generated by Three-Dimensional Landslides. JGR-Oceans, v. 110, C03006, doi:10.1029/2004JC002443.

Lynett, P., Wu, T., and Liu, P (2002) Modeling wave runup with depth-integrated equations. Coastal Engineering 46: 89-107.

Park, H., Cox, D. T., Lynett, P. J., Wiebe, D. M., & Shin, S (2013) Tsunami inundation modeling in constructed environments: A physical and numerical comparison of free-surface elevation, velocity, and momentum flux. Coastal Engineering, 79, 9-21.

Suppasri A, , Koshimura S, Imamura F (2011) Developing tsunami fragility curves based on the satellite remote sensing and the numerical modeling of the 2004 Indian Ocean tsunami in Thailand. Nat Hazards Earth Syst Sci 11:173–189

Suppasri A, Mas E, Charvet I, Gunasekera R, Imai K, Fukutani Y et al. (2013) Building damage characteristics based on surveyed data and fragility curves of the 2011 Great East Japan tsunami. Nat Hazards 319–341

Synolakis, C.E., E.N. Bernard, V.V. Titov, U. Kâno˘glu, and F.I. González (2008): Validation and verification of tsunami numerical models. Pure Appl. Geophys.,165(11–12), 2197–2228

Tsunami Pilot Study Working Group (2006) Seaside, Oregon, Tsunami Pilot Study—Modernization of FEMA Flood Hazard Maps. Joint NOAA/USGS/FEMA Special Report 94

Wiebe, D.M. and Cox, D.T. (2014) "Application of Fragility Curves to Estimate Damage and Economic Loss at a Community Scale: A Case Study of Seaside, Oregon," *Natural Hazards*, 71, 2043 – 2061.